Interface-Engineered Integration of Nickel–Iron Phosphide with Carbon for Efficient and Stable Oxygen Evolution in Alkaline Media

Tao Zhou [a,‡], Zhe Liu [a,‡], Kyeounghak Kim [b], Taekyung Yu [a,]*

a. Department of Chemical Engineering, College of Engineering, Integrated Engineering Major, Kyung Hee University, Yongin 17140, Korea.

b. Department of Chemical Engineering, Hanyang University, Seoul 04763, Korea

* Correspondence: tkyu@khu.ac.kr (T.Y.)

Table S1. Geometric parameters of the Couette-Taylor reactor used in the present synthesis

Parameters	
Radius of outer cylinder (r_o)	20.78 mm
Radius of inner cylinder (r_i)	20.00 mm
Length of inner cylinder (L)	120 mm
Gap size (d)	0.78 mm
Working volume (V)	12.2 mL

Table S2. Simulated results of the Nyquist spectra of different catalysts.

Catalysts	R_s (Ω)	R_{ct} (Ω)	Errors (%)
NiFe-P@C	9.992	10.77	0.71423
NiFe LDH@C	5.765	107.7	1.6322
NiFe-P	13.83	149.6	1.1739
NiFe LDH	6.037	187	1.0309
Ni-P@C	10.6	462.2	1.0325
Fe-P@C	10.08	848.7	1.2071
NiFe@C	13.13	127.4	1.6099
NiFe-P@C-200	9.982	20.86	0.3954
NiFe-P@C-100	10.35	26.29	0.8605
NiFe-P@C-50	9.5	43.3	1.391

Table S3. Comparison of OER activity and stability in 1.0 M KOH of previously reported transition metal-based electrocatalysts.

Catalysts	Current Density (mA cm^{-2})	Overpotential (mV)	Tafel slope (mV dec^{-1})	References
NiFe-P@C	10	233	44.8	This work
FeCoNi-P/NF	10	239	55.87	J. Alloys Compd., 960 (2023) 170493
NiFe-LDH-carbon nanospheres	10	264	67.8	Int. J. Hydrog. Energy, 190 (2025) 152234
Co_2P-1/Ni_2P-1@NF	10	310	69.9	J. Alloys Compd., 907 (2022) 164479
NCP-10/NF	10	293	84	Appl. Catal., B, 327 (2023) 122444
Co-B/NiFe-LDH	10	244	56	Electrochim. Acta 539 (2025) 147094
NiSP/NF	10	281	68.51	J. Alloys Compd., 895 (2022) 162675
FeSe/Co_2P/NF	10	235	65.6	J. Mater. Chem. A, 11 (2023) 8330-8341
NiFe-LDH/SnS	10	310	53.6	Appl. Surf. Sci., 623 (2023) 157079
NiFe-LDH-S	10	297	56.4	Inorg. Chem. Front., 9 (2022) 3598-3608
$Ni_2P/FeP_4@TiO_2$	10	260	55	Chem. Eng. J. 504 (2025) 158701
$NiFe_{alloy}$/NiFeN	10	245	20.08	J. Mater. Chem. A 13 (2025) 13440-13456
Cu-Co-P/NF	10	334	40	J. Electroanal. Chem., 939 (2023) 117478

$Ni_{0.75}Fe_{0.25}$-Al	10	279	38	ACS Catal., 15 (2025) 1123-1134
LCO-NiFe-C_3N_4	10	251.4	60.8	J. Colloid Interface Sci., 680 (2025) 787
$Ni_{2.5}Fe_{2.5}$-P/$Ti_3C_2T_x$	10	290	72.3	J. Colloid Interface Sci., 689 (2025) 137263
NiFeP-rGO	10	250	68.4	J. Colloid Interface Sci., 638, (2023), 801-812

16

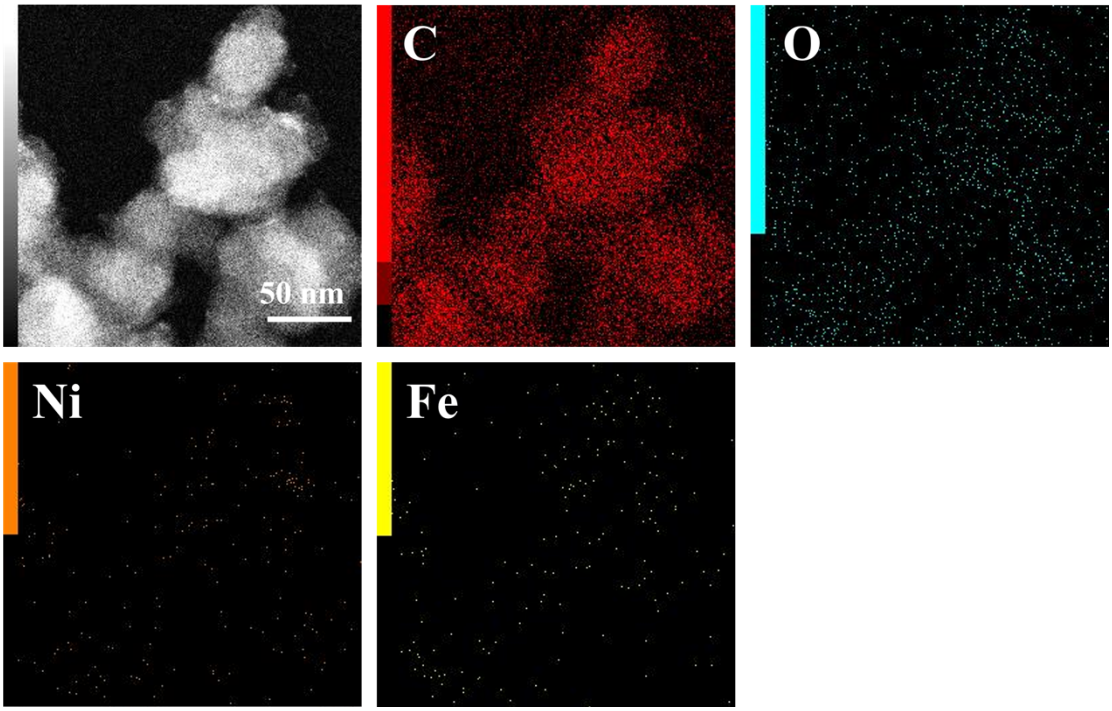

Figure S1. Elemental mapping images of C, O, Ni, and Fe in the NiFe LDH@C.

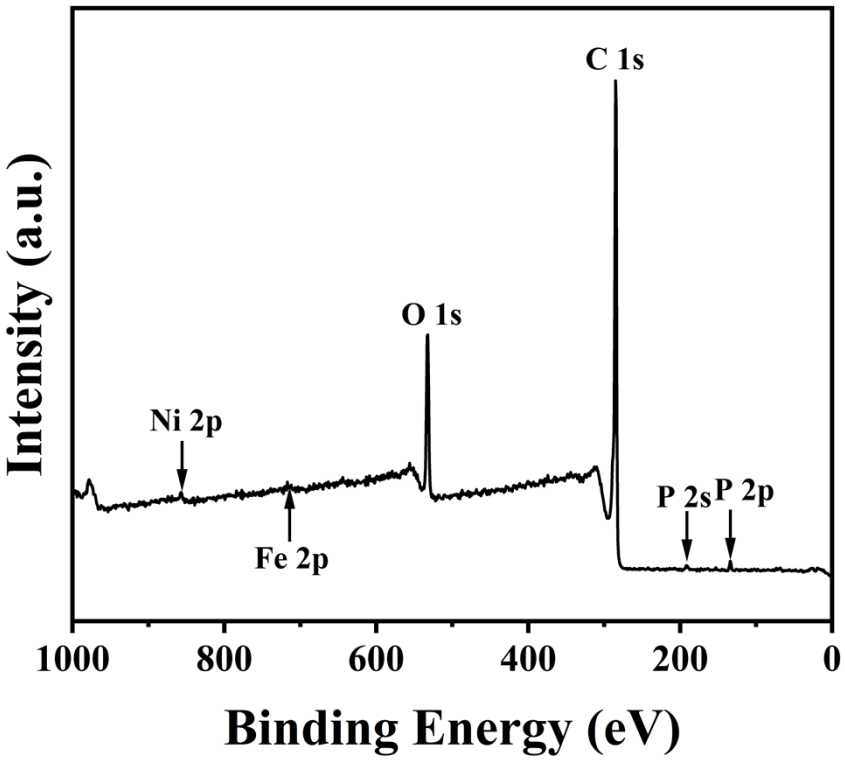

Figure S2. XPS spectrum of the NiFe-P@C.

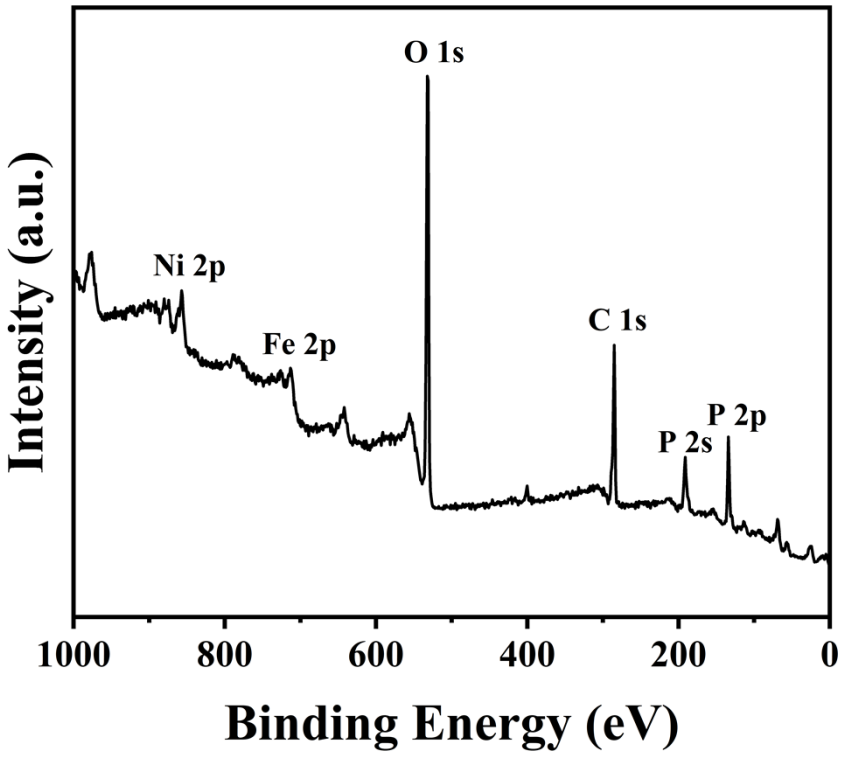

23

24 **Figure S3**. XPS spectrum of the NiFe-P.

25

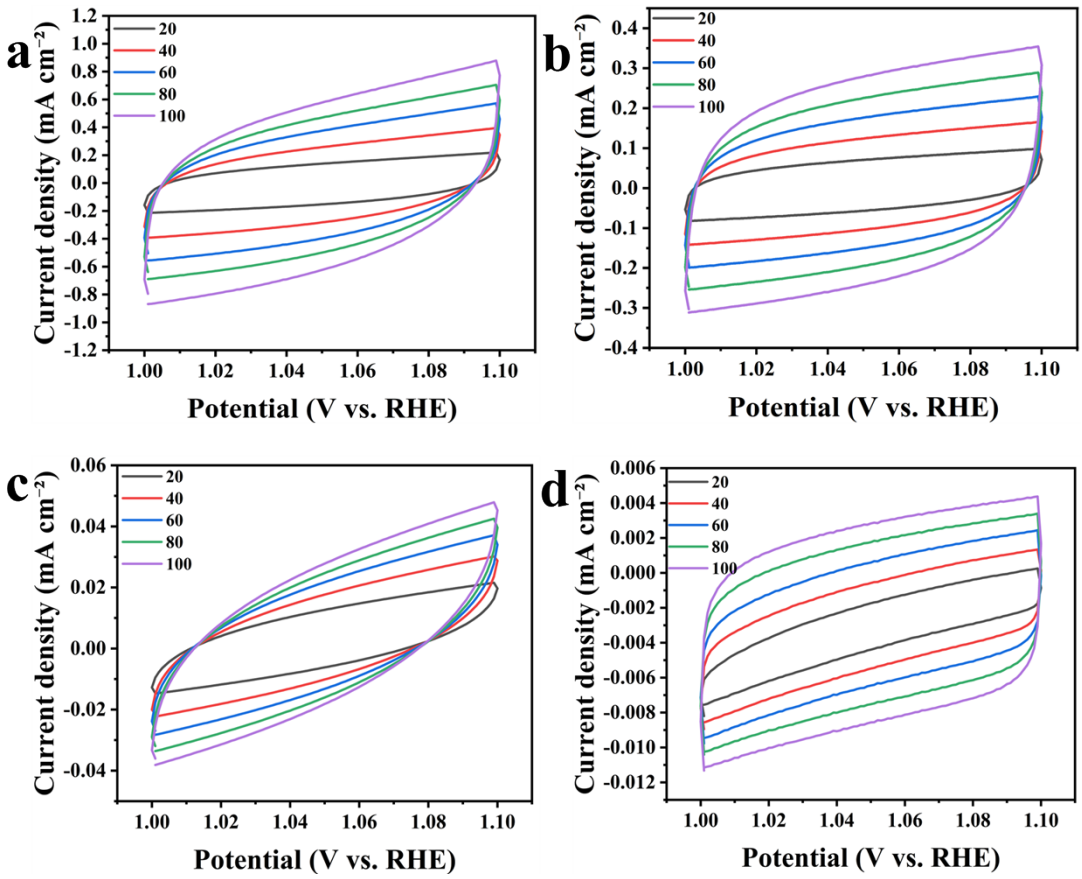

Figure S4. Cyclic voltammographs for the (a) NiFe-P@C, (b) NiFe LDH@C, (c) NiFe-P, and (d) NiFe LDH in the region of 1-1.1 V vs. RHE in 1M KOH, respectively.

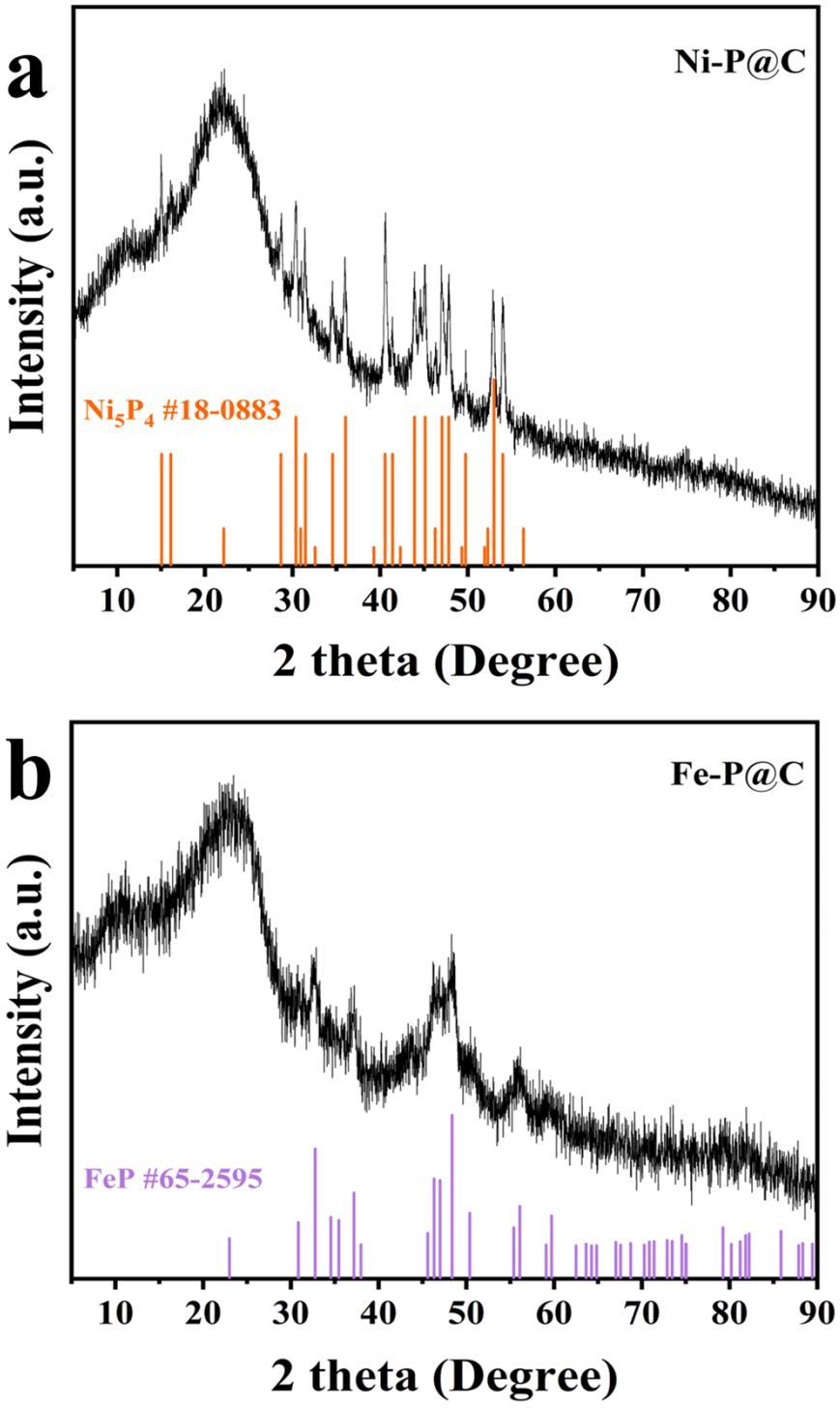

Figure S5. XRD patterns of the (a) Ni-P@C and (b) Fe-P@C, respectively.

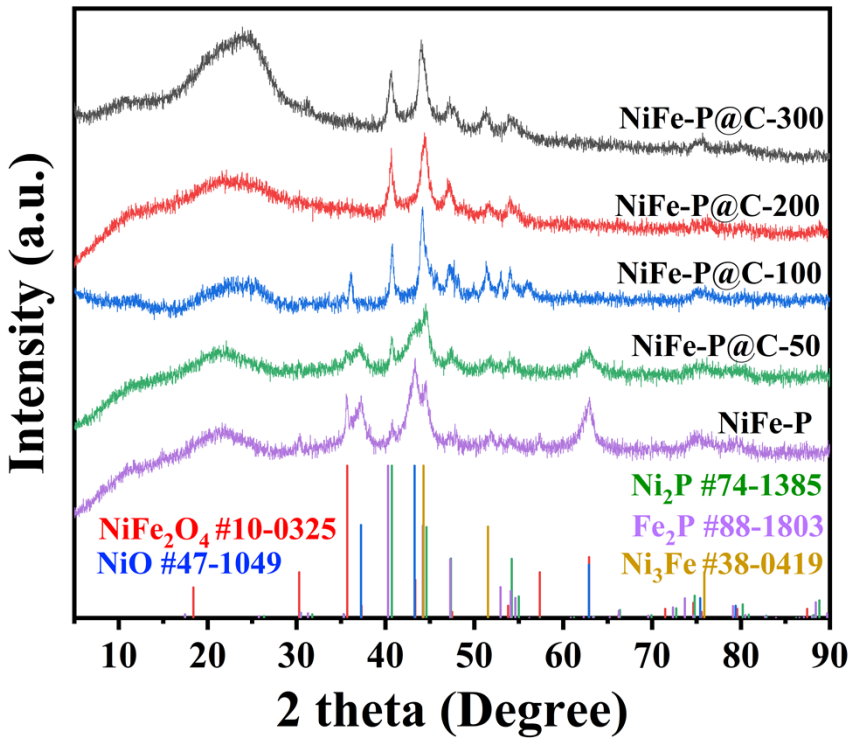

32

33 **Figure S6.** XRD patterns of the NiFe-P@C-300, NiFe-P@C-200, NiFe-P@C-100,

34 NiFe-P@C-50, and NiFe-P, respectively.

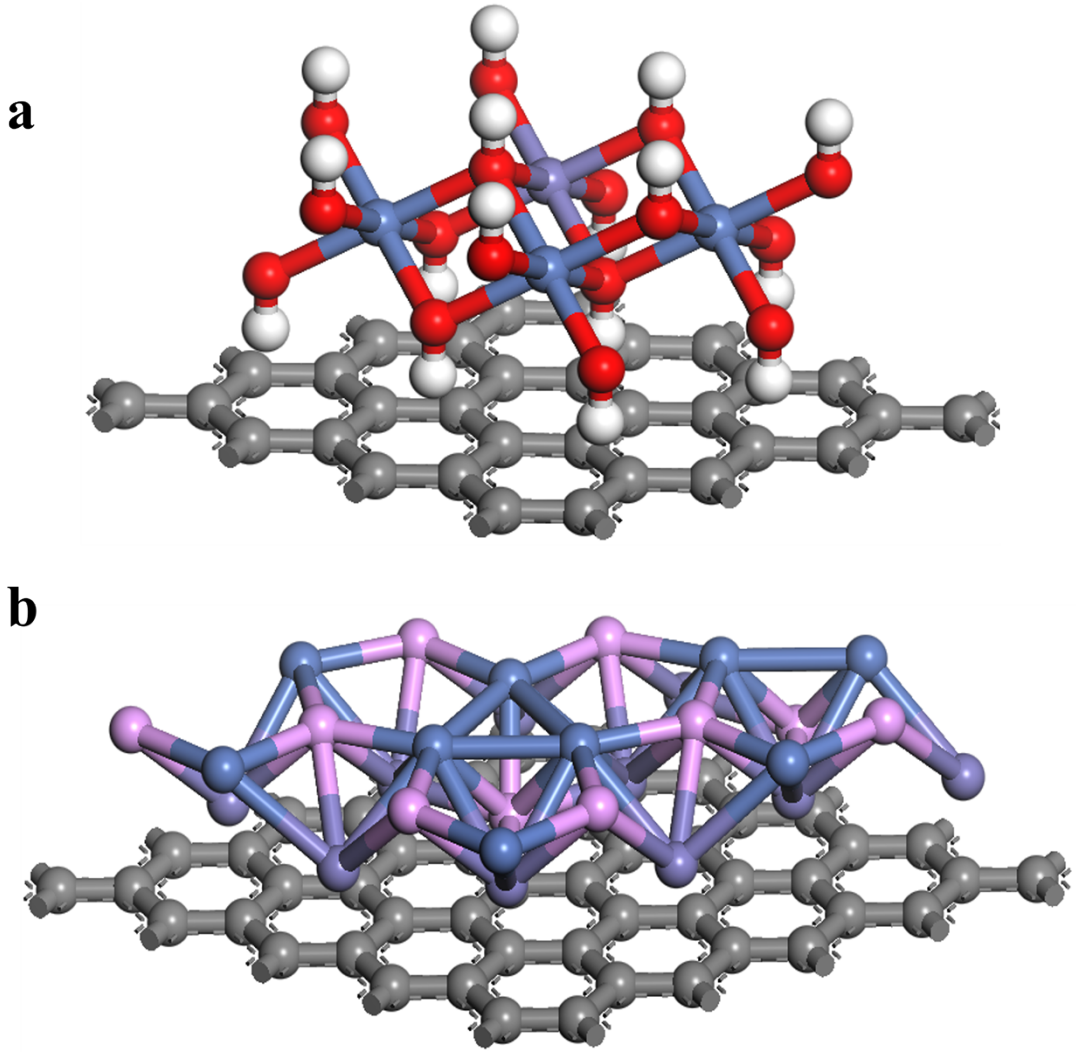

Figure S7. The optimized atomic models of the (a) NiFe LDH@C and (b) NiFe-P@C, respectively.